Chemical Engineering Journal 500 (2024) 156629

Contents lists available at ScienceDirect

Chemical Engineering Journal

journal homepage: www.elsevier.com/locate/cej

Biofilm mass transfer and thermodynamic constraints shape biofilm in trickle bed reactor syngas biomethanation

Estelle M. Goonesekera [a], Antonio Grimalt-Alemany [a], Eirini Thanasoula [a], Hassan F. Yousif [a], Sarah L. Krarup [a], Maria Chiara Valerin [b], Irini Angelidaki [a,*]

[a] Department of Chemical and Biochemical Engineering, Technical University of Denmark, 228A Søltofts Plads, 2800 Kgs. Lyngby, Denmark
[b] Department of Biology, University of Padova, Via U. Bassi 58/b, 35121 Padua, Italy

ARTICLE INFO

Keywords:
Syngas biomethanation
Trickle bed reactor
Mixed microbial consortia
Biofilm
Thermodynamics
Carbon capture

ABSTRACT

Syngas (H_2, CO_2, CO) produced thermochemically from lignocellulosic biomass is an underexploited source for resource recovery and valorisation through its biological conversion for the production of a wide range of chemicals and fuels. Syngas biomethanation is one such promising bioconversion pathway, displaying interesting features such as high conversion efficiency and product selectivity, as methane is the sole product of the process. The biological conversion of syngas to high purity biomethane is still typically associated with a number of challenges related to the syngas composition, CO toxicity, and gas–liquid mass transfer limitations. In this work, the syngas biomethanation process carried out in trickle bed reactors was investigated at its boundary conditions to explore the limits of the process, focusing on syngas composition and mass-transfer conditions potentially limiting process performance. The process was found to be robust when exposed to CO excess, but highly sensitive to H_2 excess, which caused severe inhibition even under small amounts of excess H_2. This implies that biomethane purity comparable to natural gas can be achieved by addition of renewable H_2, but this requires precise control to avoid process failure. Modulating the liquid recirculation rate and gas residence time allowed for a maximum methane productivity of 9.8 ± 0.5 mmol CH_4 h^{-1} $L_{reactor}^{-1}$ with full conversion of H_2 and CO at a gas residence time of 1 h. Nevertheless, increasing the gas–liquid mass transfer with increasing liquid recirculation rate did not lead to increased methane productivity, which suggested additional rate-limiting bottlenecks in the process. Careful investigation of other factors potentially limiting the process led to the conclusion that diffusive transport of syngas components in the biofilm was the main bottleneck of the process. This diffusive limitation leads to a scenario of severe substrate scarcity in the biofilm phase that conditions the thermodynamic feasibility of the different biochemical reactions involved in syngas biomethanation. In turn, these thermodynamic constraints were found to drive the stratification of microbial groups and sequential consumption of syngas components along the height of the reactor.

1. Introduction

Gasification and pyrolysis are thermochemical treatments applied to dry, woody biomass for which anaerobic digestion is unsuitable. They are more advantageous than incineration especially when alternative products to electricity and heat are desired [1,2]. Their products are biochar, bio-oil and syngas (or synthesis gas). Syngas is mainly composed of hydrogen (H_2), carbon monoxide (CO), carbon dioxide (CO_2), and methane (CH_4). It also contains traces of sulphide compounds, nitrogen compounds, condensable organics, and tars [3]. Currently, it is burned to produce heat and electricity on-site, but syngas can be converted thermo-catalytically and biologically into other products, such as methane and alcohols. Its conversion into methane (CH_4) is particularly interesting because it allows the transformation of syngas into a stable and versatile energy carrier that is miscible with natural gas in already existing infrastructures [4].

Biological conversion of syngas to methane, also called syngas biomethanation, is commonly carried out by a mixed microbial community and encompasses a series of interrelated metabolic interactions carried out by different microbial trophic groups. The main reactions are hydrogenotrophic and aceticlastic methanogenesis, carboxydotrophic acetogenesis and hydrogenogenesis, homoacetogenesis, and syntrophic

* Corresponding author.
E-mail address: iria@kt.dtu.dk (I. Angelidaki).

https://doi.org/10.1016/j.cej.2024.156629
Received 1 July 2024; Received in revised form 3 October 2024; Accepted 10 October 2024
Available online 11 October 2024

acetate oxidation [5]. Which pathways dominate depend on operational conditions, most notably temperature. In mesophilic conditions, pathways with acetate as an intermediary dominate, whereas H_2 is the principal intermediary in thermophilic conditions [6]. The microbes are the biocatalysts of the process and give biological conversion distinct advantages over thermo-catalytic conversion. This includes taking place at milder temperatures (37–75 °C) and atmospheric pressure and relying on inexpensive biocatalysts. Moreover, biological conversion is more robust to contaminants such as hydrogen sulphide, which is known to poison catalysts used for thermo-catalytic conversion processes [7]. Furthermore, syngas composition is variable and depends on both waste properties and the pyrolysis or gasification operating conditions [1]. Thermo-catalytic conversion requires a specific and invariable syngas composition (fixed H_2:CO ratio), while biological conversion is more flexible, as all electron donors (H_2 and CO) contained in syngas can be fully converted independently of the H_2:CO ratio. Nonetheless, biological syngas conversion does face a series of challenges that remain to be studied and addressed in detail.

One such challenge is related to syngas composition, which depends on multiple parameters such as biomass composition, operational conditions, oxidizing agents, etc., and may also vary substantially during continuous operation. On the one hand, high CO content has been reported to cause inhibition due to its toxicity to microorganisms in suspended cultures, whereas robustness to CO was reported when microbes were spatially arranged in protective structures such as granules [8–10]. CO toxicity is nevertheless still mentioned as a challenge to syngas biomethanation [1,11,12]. On the other hand, syngas is relatively energetically poor and typically lacks reducing equivalents, i.e. H_2, to fully convert the CO and CO_2 to gas with a high CH_4 content [1]. Interestingly, this lack of H_2 presents an opportunity to use syngas biomethanation for storage of energy during periods of peak renewable energy production. The electricity from renewable overproduction could be converted to H_2, which can be added to the syngas biomethanation process to achieve full conversion to CH_4 [13,14]. However, stoichiometric excess of H_2 has been shown to be detrimental to the process because it interferes with the consumption of CO, one of the key reactions in syngas biomethanation [13]. Under thermophilic conditions, CO is typically transformed with H_2O into a mixture of H_2 and CO_2 [15], but this can be hampered if the H_2 concentration is too high, because the transformation of CO to H_2 becomes thermodynamically unfeasible [13]. This raises the need to further study the effect of syngas composition on syngas biomethanation performance. Key aspects to be revisited are the possibility of the toxicity of CO in the inlet syngas inhibiting (or not) the biofilm's capacity to convert the syngas, and the potential for (and extent of) thermodynamic inhibition of CO conversion when the inlet syngas contains small stoichiometric excesses of H_2.

Another challenge faced by biological syngas conversion is achieving effective mass transfer from the gas phase (where the carbon and electron sources are) to the liquid phase and the solid (biofilm) phase, where biochemical reactions take place. Trickle bed reactors (TBRs) have been proposed as the best option to maximise gas–liquid mass transfer [16,17], so far regarded as the key limiting parameter in gas fermentation processes [5]. TBRs are gas phase reactors filled with high specific surface area packing material over which liquid medium is trickled. The packing material and trickling simultaneously promote gas–liquid mass transfer and the formation of biofilm, which allows the retention of slow growing anaerobes in the reactor [18]. Although biofilm gives trickle bed reactors an advantage in gas fermentation, the compounds in the gas phase do need to be transported within the biofilm to reach the microbes that will eventually consume them. This transport occurs by diffusion, and at rates much slower than those reported for gas–liquid mass transfer [19]. It is thus plausible to hypothesise that gas–liquid mass transfer is not the sole bottleneck in the syngas biomethanation process, and that increasing the liquid recirculation rate will only have a minor effect on process performance.

As the syngas moves along the bed, its constituents are transformed according to the catabolic reactions of the microbiome into methane or into intermediate products that are subsequently converted into methane by other microorganisms. The main catabolic reactions taking place at thermophilic conditions are carboxydotrophic hydrogenogenesis (the biological gas-shift reaction) and hydrogenotrophic methanogenesis. Under certain conditions, carboxydotrophic acetogenesis and syntrophic acetate oxidation can also take place [6]. It is hypothesised that the partial pressure of the constituents at each position in the reactor influence which catabolic reactions are thermodynamically feasible. This, in turn, is thought to drive the selection of those microorganisms that can carry out the energy-giving reactions in that context, leading to a higher abundance at that height. Consequently, the mixed microbial community is expected to show a level of stratification within the reactor driven by its metabolic capabilities and the circumstances provided by both gas composition and the rate of gas flow.

The aim of this work is thus to explore the limits of the syngas biomethanation process, focusing on the identification of the main bottlenecks of the process in trickle bed reactors. This work addresses the gas composition challenges outlined above, namely the possible toxicity of CO and the effect of excess H_2. The parameters influencing gas–liquid mass transfer are also studied with the specific aim to observe if an increase in liquid recirculation rate could improve syngas conversion. Finally, the reactor's microbiome at different heights is analysed to describe the distribution of microorganisms and their interactions within the bed.

2. Materials and methods

2.1. Reactor setup and characterisation

A 1 L borosilicate glass trickle bed reactor (TBR; 80 mm diameter, 540 mm height) filled with K1 PE/PP (Evolution Aqua, UK) packing material was operated co-currently at thermophilic conditions (55 ± 1 °C). The residence time distribution was measured using a standard tracer test method [20]. NaCl solutions of 0.01, 0.1 and 1 M were used to check consistency. Liquid was introduced at the top of the reactor and the conductivity was measured at the outlet. The relative concentration (C/C_0) was calculated for each time step and plotted over time. This residence time distribution was then integrated to obtain the overall residence time.

$$\theta = \int_0^t W(t)\,dt \tag{1}$$

where θ is the residence time, $W(t)$ is the relative concentration residence time distribution, and t is the final sampling time point. This procedure was repeated for liquid recirculation rates of 40, 120 and 200 mL min^{-1} to establish the relationship between liquid recirculation rate and liquid residence time.

The volumetric mass transfer coefficient (k_La) was also measured for different liquid recirculation rates. Synthetic syngas (Air Liquide, Denmark) and water (at 55 ± 1 °C) were introduced co-currently at the top of the reactor and collected at the bottom with no recirculation of any streams to quantify the effective gas-to-liquid mass transfer along the bed of the reactor. Liquid samples (5 mL) were carefully collected at the outlet avoiding the collection of gas bubbles and were stored in 10 mL sealed serum bottles. The saturation concentration of the gases was determined in a 250 mL serum bottle with 100 mL working volume of distilled water and a 150 mL syngas headspace. The bottle was placed in an incubator at 55 °C overnight, after which two 5 mL liquid samples were taken and stored in 10 mL sealed serum bottles. The 10 mL serum bottles were heated to 100 °C for 30 min to strip the compounds of interest to the gas phase, after which the headspace composition was measured using gas chromatography. The mass transfer of a compound i can be expressed as:

$$\frac{C_i}{d\theta_l} = k_L a(C_i^* - C_i) \quad (2)$$

where C_i is the concentration of compound i at the outlet of the reactor, C_i^* is the saturation concentration of compound i, and θ_l is the hydraulic residence time. Equation (2) was then linearised to calculate the k_La by plotting $\ln(1 - C_i/C_i^*)$ against the residence time. The slope between this point and the inlet concentration (0 mM) is the k_La. This method assumes that the outlet concentration is at steady state, the liquid phase follows plug flow, and the liquid holdup is constant along the bed. Five replicate samples were taken for each liquid recirculation rate.

2.2. Gas residence time, liquid recirculation and trace element supply

The reactor was inoculated with syngas-adapted anaerobic digestion digestate previously adapted to growth on syngas. The growth medium was liquid fraction of digestate (Solrød Biogas Plant, Denmark) degassed at 55 °C, where solids were removed using a 1 mm sieve. To avoid ammonium inhibition, the liquid fraction of digestate was diluted 1:2 with tap water, resulting in 1.1 ± 0.02 g NH_4^+-N L^{-1}. The bicarbonate was stripped from the liquid fraction of digestate, using acidification with HCl (Sigma-Aldrich, USA) and N_2 bubbling (Air Liquide, Denmark), to be able to accurately quantify CO_2 balance of the reactor, since CO_2 is present in syngas. The initial pH of the liquid influent was adjusted with phosphate buffer to avoid large fluctuations in the pH of the process. In some conditions the liquid fraction of digestate was supplemented with 15 mL L^{-1} of double modified Wolin's mineral solution (DSMZ medium S5902, Germany), 0.08 g L^{-1} sodium sulphide, and 0.01 g L^{-1} sodium tungstate. The medium was held in a 1 L liquid reservoir and continuously recirculated from the reservoir to the top of the reactor using a peristaltic pump (Watson-Marlow, UK), from where it trickled through the packed bed. The reactor was operated in semi-continuous mode by manually replacing medium daily to keep a constant liquid volume and a hydraulic retention time of 20 days. The TBR was operated in co-current mode (see Fig. 1), with synthetic syngas (Air Liquide, Denmark) fed by peristaltic pump (BT100-2J YZ1515x, Longer, UK) from the top of the reactor. Exit gas flow was measured by a gas meter. The TBR was equipped with sampling ports for gas measurement at the gas inlet and before the gas meter, a liquid sampling port in the liquid reservoir, and three sampling ports for gas and packing material sampling along the height of the column.

The gas residence time (GRT) was calculated as the empty bed residence time:

$$GRT = V_{EB}/Q_{in} \quad (3)$$

where V_{EB} is the volume of the empty reactor and Q_{in} is the inlet flow of syngas. Sampling took place daily or twice-daily. Gas samples were taken using a gas-tight syringe (Hamilton ® SampleLock syringe 1750SL volume 0.5 mL, needle size 22 ga (bevel tip), needle L 51 mm, Hamilton, USA). Liquid samples were taken from the liquid reservoir, centrifuged and the supernatant frozen until analysis. An experimental condition was considered to have reached steady state when the difference in CH_4 content was less than 5 % on three consecutive days. Each measurement on a consecutive day at steady state was considered an experimental replicate and each condition remained at steady state for at least four days.

The performance of the syngas biomethanation reactor was assessed in terms of net conversion efficiency and CH_4 productivity. Conversion efficiency was calculated as:

$$Conversion\ efficiency = \frac{Q_{g,i,in} - Q_{g,i,\ out}}{Q_{g,i,in}} \quad (4)$$

where $Q_{g,i,in}$ is the inlet flow of compound i (in the gas phase), and $Q_{g,i,out}$ is its outlet flow. CH_4 productivity was calculated as:

$$CH_4 productivity = \frac{Q_{g,CH_4,out} - Q_{g,CH_4,in}}{V_{EB}} \quad (5)$$

where $Q_{g,CH_4,out}$ and $Q_{g,CH_4,in}$ are the outlet and inlet flow of CH_4, respectively, and V_{EB} is the volume of the empty reactor volume. OriginPro (version 2023, OriginLab Corporation, USA) was used for statistical analysis of the results.

2.3. Experimental conditions

2.3.1. Gas composition

The proportions of H_2, CO and CO_2 in syngas determine the CH_4 content that can be produced from it. A useful way to summarise the composition is the ratio of electron donor (H_2 and CO) to electron acceptor (CO and CO_2) as in Asimakopoulos et al. [13]. CO is both an electron donor and acceptor because through the biological water–gas shift reaction CO and H_2O result in H_2 (an electron donor) and CO_2 (an electron acceptor). The e-donor/e-acceptor ratio necessary for a complete conversion of all syngas components to CH_4 is 4. These experimental conditions are summarised in Table 1. The gas residence time was 3 h, the liquid recirculation rate was 20 mL min^{-1}, and the recirculated liquid volume was 1 L.

2.3.2. Gas residence time, liquid recirculation and trace element supply

The limiting factor of syngas conversion in trickle bed reactors was investigated with the experimental conditions summarised in Table 2. The aim was to discern gas–liquid mass transfer limitation from nutrient limitation and observe if any other bottlenecks were present. The TBR

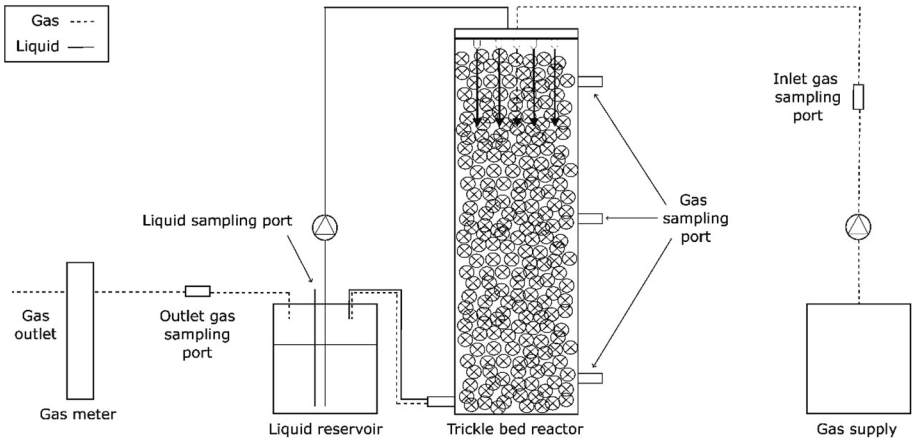

Fig. 1. Experimental setup of the trickle bed reactor for syngas biomethanation.

Table 1
Experimental conditions for the study of the effect of syngas composition expressed in percentage, and ratio of electron donor to electron acceptor [13], together with the overall and steady state duration of each condition.

Condition	Gas composition (%)				e^- donor/e^- acceptor	Duration (d)	
	H_2	CO	CO_2	N_2		Total	Steady state
Control	65	16.7	13.1	5.2	2.7	17	9
High CO	33.3	40	16.7	8.33	1.2	13	7
High H_2	74.3	12.0	8.6	5.1	4.1	7	4

Table 2
Experimental conditions for the study of the bottleneck in syngas conversion in trickle bed reactors: Gas residence time, liquid recirculation rate and application of trace element supplementation (15 mL L^{-1} double modified Wolin's mineral solution, 0.08 g/L sodium sulphide, and 0.01 g/L sodium tungstate), together with the overall and steady state duration of each condition.

Gas residence time (h)	Liquid recirculation rate (mL min^{-1})	Trace element supplementation	Duration (d)	
			Total	Steady state
1.5	20	No	13	9
1	20	No	14	5
1.5	280	No	14	7
1	280	No	15	5
1.5	20	Yes	9	3
1	20	Yes	7	5
0.75	20	Yes	10	5
0.75	280	Yes	16	5

was operated at different gas residence times and liquid recirculation rates, and the effect of the addition of trace elements was tested. The gas composition was 65 % H_2, 16.7 % CO, 13.1 % CO_2 and 5.2 % N_2 (see Control in Table 1), and the recirculated liquid volume was 1 L.

2.4. Analytical methods

Biomass content in the liquid phase and attached to the carriers was quantified by measuring total solids [21]. The biomass from the carriers was detached by shaking in 20 mL phosphate buffer saline 1x (PBS, 137 mM NaCl, 2.7 mM KCl, 10 mM Na_2HPO_4, 1.8 mM K), the carriers removed, the suspension centrifuged, and the supernatant discarded. Gas composition was monitored using gas chromatography (GC-TRACE 1310, ThermoFisher Scientific, USA). A Thermo (P/N 26004-6030) (ThermoFisher Scientific, USA 30 m length, 0.320 mm inner diameter, and 10 μm film thickness) was used for CH_4 and CO_2, and an HP-Molesieve column (Agilent Technologies, USA, length 30 m, diameter, 0.53, film 50 μm) was used for H_2, CO, and CH_4. The injection volume was 0.2 mL. Volatile fatty acids were measured by gas chromatography (Agilent 7890A, Agilent Technologies, US) equipped with a flame ionization detector (FID) and SGE capillary column (30 m length, 0.53 mm inner diameter, film thickness 1.00 μm) with helium as carrier gas. A detailed description can be found in Giangeri et al. [22]. pH was monitored daily (Mettler Toledo LE407, Switzerland) and manually adjusted with NaOH (Sigma-Aldrich, USA) to 7 if values below 6.8 were observed.

2.5. Microbial community characterisation

After each steady state, biofilm samples were taken by opening the sampling ports along the column and removing four carriers with tweezers, and then replacing them with new carriers. Suspended samples were taken from the liquid reservoir. The carriers were directly stored at −20 °C, while the suspended samples were first centrifuged, and the supernatant discarded before freezing. The samples were subsequently used for 16S rRNA sequencing. Prior to DNA extraction and 16S rRNA sequencing, the samples were thawed, placed in 20 mL phosphate buffer saline 1x (PBS, 137 mM NaCl, 2.7 mM KCl, 10 mM Na_2HPO_4, 1.8 mM KH_2PO_4), and vortexed to release the biofilm. Once the biofilm was detached, the carriers were removed, the suspension centrifuged, and the supernatant discarded. DNA was extracted and purified using the DNeasy® PowerSoil® Pro Kit (QIAGEN 181 GmbH, Germany) following manufacturer instructions and with an additional cleaning step [23]. DNA quantity was determined using a Qubit fluorometer (ThermoFisher Scientific, USA). Polymerase Chain Reaction (PCR) amplification of the 16S rRNA hypervariable V4 region was carried out with the primers F515/R806 [24]. Library preparation was performed with the Nextera DNA Flex Library Prep Kit (Illumina Inc, San Diego, CA) and gene amplicons were sequenced with the platform NovaSeq at the NGS facility of the Biology Department of the University of Padova, Italy. Raw sequences were deposited in the NCBI SRA database with BioProject ID PRJNA1112761. Raw reads were primer-trimmed with cutadapt, discarding all untrimmed reads [25]. Trimmed reads were quality-filtered, denoised and merged using DADA2 within the Qiime2 pipeline [26]. The taxonomic assignment to amplicon sequence variants (ASVs) was performed using the classify-sklearn algorithm and a taxonomic classifier trained on the MiDAS 4.81 database using fit-classifier-naive-bayes algorithm [26,27]. Downstream analyses on ASVs were performed using the Phyloseq 1.42.0 [28], Vegan 2.6-4 [29] and ggpubr 0.6.0 [30] packages in R version 4.2.2 [31].

2.6. Thermodynamic analysis

The predominant reactions in the syngas biomethanation process under the conditions in this study are summarised in Table 3: hydrogenotrophic methanogenesis, carboxydotrophic hydrogenogenesis and syntrophic acetate oxidation. The interactions between them are evaluated using the Gibbs free energy change ($\Delta_r G'_T$) as described in Grimalt-Alemany et al. [6] and the thermodynamic potential factor (F_T) proposed by Jin and Bethke [32].

$$F_{T,i} = 1 - \exp\left(\frac{-\Delta_r G'_{T,i} - Y_{ATP,i}\Delta G_P}{\chi RT}\right) \quad (6)$$

$$\Delta_r G'_T = \Delta_r G^{\circ}_T + RT\ln\frac{[C]^c[D]^d}{[A]^a[B]^b} \quad (7)$$

where $Y_{ATP,i}$ is the ATP yield of the metabolic reaction, ΔG_P is the Gibbs free energy of ATP synthesis, χ is the average stoichiometric number (see Table 3), R is the universal gas constant, and T is the temperature. $\Delta_r G'_T$ corrects the Gibbs free energy of the reaction ($\Delta_r G^{\circ}_T$) by taking into account the concentration in the phase under evaluation and the effects of temperature and ionic strength by correcting the Gibbs free energy of formation [33]. ΔG_P has been reported to range between 40 and 50 kJ/mol ATP [32], and the value of 45 kJ/mol ATP is used unless otherwise

Table 3
Representative biochemical reactions, their ATP yield, and the average stoichiometric number used in the thermodynamic potential factor (F_T) calculations.

	Hydrogenotrophic methanogenesis	Carboxydotrophic hydrogenogenesis	Syntrophic acetate oxidation
Reaction	$4\ H_2 + CO_2 \rightarrow CH_4 + 2\ H_2O$	$CO + H_2O \rightarrow H_2 + CO_2$	$CH_3COOH + 2\ H_2O \rightarrow 4\ H_2 + 2\ CO_2$
ATP yield (mol/mol product)	0.5	0.33	0.33
Average stoichiometric number (χ)	2	2	1
Reference	[34]	[6,37]	[38]

indicated. Hydrogenotrophic methanogenesis was assumed that to be performed by species without cytochromes that translocate $6Na^+$ across the membrane (investing 1 mol ATP in acetate activation), had an ATP synthesis stoichiometry of $4Na^+$ per ATP formed [34], and whose rate determining step was the translocation of Na^+ by the methyl transferase complex. Carboxydotrophic hydrogenogenesis was assumed to translocate one H^+ per mol of CO across the membrane through an energy conserving hydrogenase and use an ATP synthesis stoichiometry of $3H^+$ per ATP synthesised [6,35]. Syntrophic acetate oxidation was assumed to use an ATP synthesis stoichiometry of $3H^+/Na^+$ per ATP formed [36].

As a preliminary exploration, the thermodynamic feasibility of the reactions in Table 3 were evaluated for a broad range of concentrations ($1{\cdot}10^{-6}$ to $1{\cdot}10^{-4}$). The gas composition, the microbial community and the liquid phase concentration profile along the height were then compared with these results to further explain the observed profiles with thermodynamic insights. Liquid phase concentrations were calculated based on the assumption that the uptake rate of syngas components between two sampling points ($q_i(\Delta h)$) must be equal to the mass transfer rates, which can be used to determine the dissolved concentrations fulfilling that equality:

$$\begin{cases} q_i(\Delta h) = k_L a\left(C_{g,i}(h_j) - \dfrac{C_{l,i}(h_j)}{K_{H,i}}\right) \\ q_i(\Delta h) = \dfrac{C_{g,i}(h_{j-1}) - C_{g,i}(h_j)}{\theta_g(\Delta h)} \end{cases} \quad (8)$$

where $C_{g,i}$ is the gas phase concentration, $K_{H,i}$ is Henry's law constant, and $C_{l,i}(h_j)$ is the concentration of compound i in the liquid phase at a height j. The gas residence time between each sampling height $\theta_g(\Delta h)$ was calculated using N_2 balance:

$$\theta_g(\Delta h) = \frac{C_{g,N_2}(h_j)\, V_{EB}}{Q_g(h_{j-1})\, C_{g,\,N_2}(h_{j-1})} \quad (9)$$

where C_{g,N_2} is the N_2 content in the gas at a specified height.

3. Results and discussion

3.1. The effect of syngas composition

CO toxicity to methanogens is still mentioned as a challenge in syngas biomethanation [1,11,12] due to the CO toxicity reported in suspended cultures. This is despite previous studies documenting the robustness of microbial communities previously adapted to high CO partial pressures, especially in spatial configurations such as granules or biofilm [8,9,11]. Previous studies of syngas biomethanation in TBRs in particular do not show evidence of CO toxicity to microorganisms, but they all use a CO content no higher than 30 % (i.e. a partial pressure of 0.3 atm) [12,13,15,39]. Using a higher content of CO (40 % or 0.4 atm partial pressure) could contribute to reframing the challenge posed by CO inhibition. H_2 accumulation has been reported to inhibit the activity of carboxydotrophic hydrogenogenic bacteria converting CO into H_2 and CO_2 [11,13,40]. Accounting for this potential H_2 inhibition, real-world syngas biomethanation plants targeting biomethane production (where the pyrolysis gas or syngas produced varies in composition over time) may find it challenging to adjust the supply of exogenous H_2 without exceeding the stoichiometric needs of raw syngas (with a theoretical maximum of 4 e-donor/e-acceptor). Therefore, the series of syngas compositions examined ranged from high CO content (1.2 e-donor/e-acceptor) to slight H_2 excess above the stoichiometric maximum (4.1 e-donor/e-acceptor), to investigate potential process failure at its boundary conditions.

Analysing the entire range of syngas compositions revealed considerable deviations from the theoretically expected reactor off-gas compositions. CO was completely consumed under high CO supply (1.2 e-donor/e-acceptor), suggesting that no significant microbial inhibition was occurring as a result of the 40 % CO content in the syngas. The off-gas CH_4 content was also in agreement with the theoretical maximum CH_4 content (Fig. 2A). The lack of CO inhibition can be explained by the fact that under mass transfer limiting conditions, the dissolved concentration of CO is well below saturation conditions, alleviating the possibility of any potential inhibition [41]. Increasing the e-donor/e-acceptor ratio to 2.7 also resulted in an outlet CH_4 content in agreement with the theoretical, with complete conversion of H_2 and CO (Fig. 2A). It should also be noted that the percentage of CO_2 dropped significantly

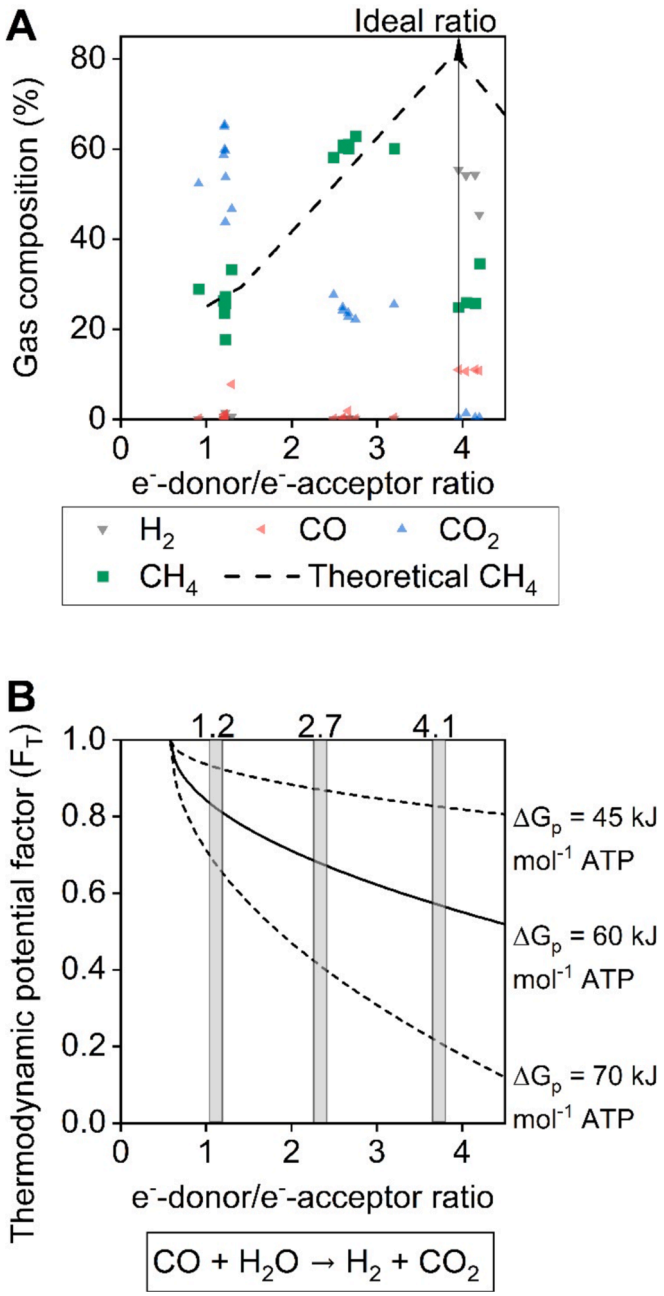

Fig. 2. A) Steady state outlet gas composition as a function of e-donor/e-acceptor ratio of the inlet gas, theoretical CH_4 content based on the e-donor/e-acceptor ratio, and stoichiometric ideal e-donor/e-acceptor ratio for complete conversion of syngas to CH_4, and B) thermodynamic potential factor as a function of e-donor/e-acceptor ratio (based on the partial pressures of CO, H_2 and CO_2 in the gas phase). The thermodynamic potential factor is presented as a range to account for the uncertainties the Gibbs free energy of phosphorylation (ΔG_P in equation 6) used. In this case, 45, 60 and 70 kJ/mol ATP were applied [38,42].

due to the higher supply of H_2, but some CO_2 remained unconverted as expected based on the e-donor/e-acceptor ratio of 2.7. Nevertheless, further increasing the H_2 supply to slightly above the stoichiometric needs (4.1 e-donor/e-acceptor) in order to convert this remaining CO_2 led to drastic process failure. The production of CH_4 and conversion of CO plummeted dramatically, likely due to the accumulation of excess H_2 and inhibition on CO conversion activity (Fig. 2A).

The conversion of CO into H_2 and CO_2 has been reported as the dominant CO-converting pathway at thermophilic conditions [6,10]. The thermodynamic potential factor was used to analyse the thermodynamics of the latter as a function of the e-donor/e-acceptor ratio of syngas. This factor indicates the strength of the thermodynamic drive for a reaction to occur [32]. The thermodynamic drive is strongest when the factor approaches 1. The factor approaching 0 is a sign of loss of drive and, thus, thermodynamic inhibition. This analysis showed a potential thermodynamic inhibition with increasing H_2 content. As shown in Fig. 2B, the thermodynamic potential factor (F_T) decreases as the e-donor/e-acceptor ratio of syngas increases, indicating a loss in thermodynamic drive for carboxydotrophic hydrogenogenesis. Therefore, at an e-donor/e-acceptor ratio of 4.1, thermodynamic inhibition is the most likely explanation for the lack of CO consumption [13,35].

The microbial community composition illustrates the catabolic reactions dominating the syngas biomethanation process under these conditions. In Fig. 3, reads mapping to hydrogenotrophic methanogens, *Methanobacterium* spp. and *Methanothermobacter* spp., reveal that the dominant methanogenic pathway is hydrogenotrophic methanogenesis. This concurs with previous research showing that H_2 is the main intermediary in thermophilic conditions [6]. Firmicutes, the phylum that includes most carboxydotrophs, e.g. *Desulfosporosinus* and *Eubacterium* spp. [43,44] are highly represented. It is most likely that these microbes produced predominantly H_2, although some acetate was also produced (between 0.2 and 16.3 mM). Acetate played a minor role in the process with only small amounts produced even in transitory state. This was nevertheless sufficient to allow the presence of acetotrophic groups. Multiple strains of syntrophic acetate oxidisers (like *Syntrophaceticus* spp.) are present in higher overall abundance than aceticlastic methanogens, represented by a single putative genus (*Methanosarcina*). This supports previous findings that hydrogenotrophic methanogenesis is the dominant methane production pathway at thermophilic conditions [6,10].

Overall, these results clearly show that risk of inhibition and process failure are not related to CO toxicity but to the thermodynamic inhibition by excess H_2. This was previously reported by Asimakopoulos et al. [13] but studied at an e-donor/e-acceptor ratio of 4.78, a substantial excess of H_2. This present study emphasises the risks of even small excesses of H_2 having an outsized effect on process viability. Consequently, these findings show that the supply of exogenous H_2 should be carefully tuned to prevent even small excess H_2 conditions due to potential variations in syngas input composition in continuous-mode operated gasification and pyrolysis reactors.

3.2. Gas residence time, liquid recirculation and trace elements supply

The performance of a trickle bed reactor (TBR), how much substrate (gaseous species) the biofilm can convert, depends on how much of this substrate can be provided to the biofilm. The movement of liquid through the bed is the main driver of the transfer of sparsely soluble compounds like H_2 and CO from the gas to the liquid phase. The liquid trickling through the packed bed of a TBR tends to follow preferential pathways, a phenomenon called channelling. This limits the mass transfer and, consequently, the productivity of the reactor. Increasing the liquid recirculation rate reportedly ameliorates channelling by ensuring that the bed is more uniformly wetted (with fewer preferential pathways), both providing nutrients to the biofilm and enlarging the surface for gas–liquid exchange [45]. This makes the impact of the liquid recirculation rate one of the key parameters to study when exploring the limits of the syngas biomethanation process.

The TBR in the current study was characterised in terms of its mass transfer capability. First, the residence time distribution was measured (Fig. 4A), followed by the gas–liquid mass transfer coefficient (k_La) for the sparsely soluble gases, H_2 and CO (Fig. 4B). The results in Fig. 4B show the relationship between the liquid recirculation rate and the gas–liquid mass transfer coefficient (k_La) under abiotic conditions, and their order of magnitude is consistent with data in the literature [46,47]. Here, an increase from 20 to 300 mL min^{-1} in liquid recirculation rate results in a 6.5- and 5-fold increase in mass transfer for H_2 and CO, respectively, the difference between species previously reported in literature [46]. This increase in mass transfer is then expected to yield increases in productivity of a similar order of magnitude.

Fig. 5 shows the process performance as a function of the gas residence time in terms of CH_4 productivity, and H_2 and CO conversion. Liquid recirculation rates of 20 and 280 mL min^{-1} were tested at gas residence times (GRT) of 1.5 and 1 h. At a GRT of 1.5 h, there were no significant differences in performance as both liquid recirculation rates

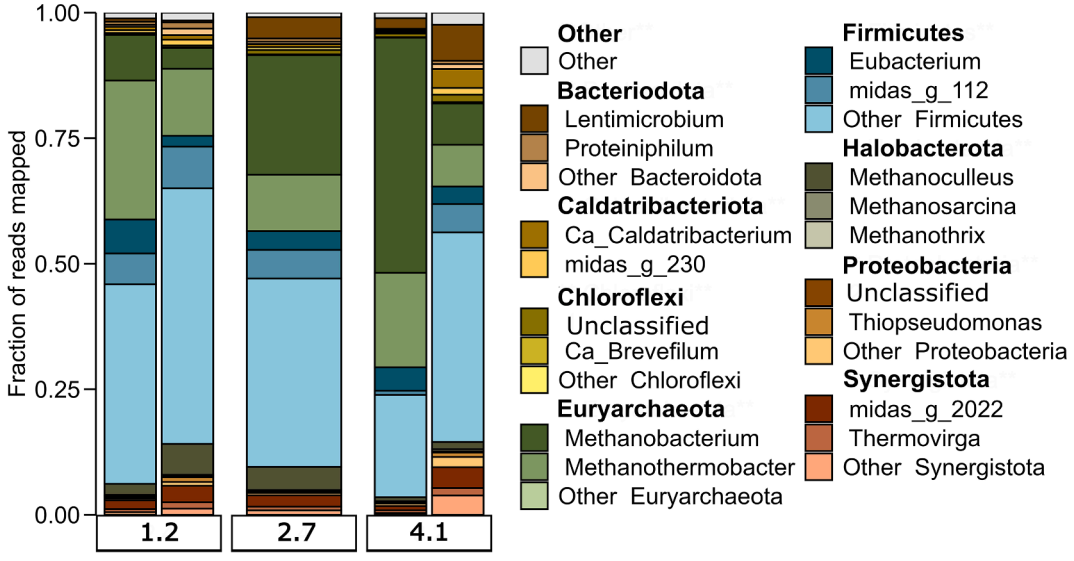

Fig. 3. Relative abundance at the middle of the reactor of dominant phyla and genera as a function of the e-donor/e-acceptor ratio. Microbial composition samples were sequenced in duplicate, except for e-donor/e-acceptor ratio 2.7, where the second replicate was not sequenced successfully.

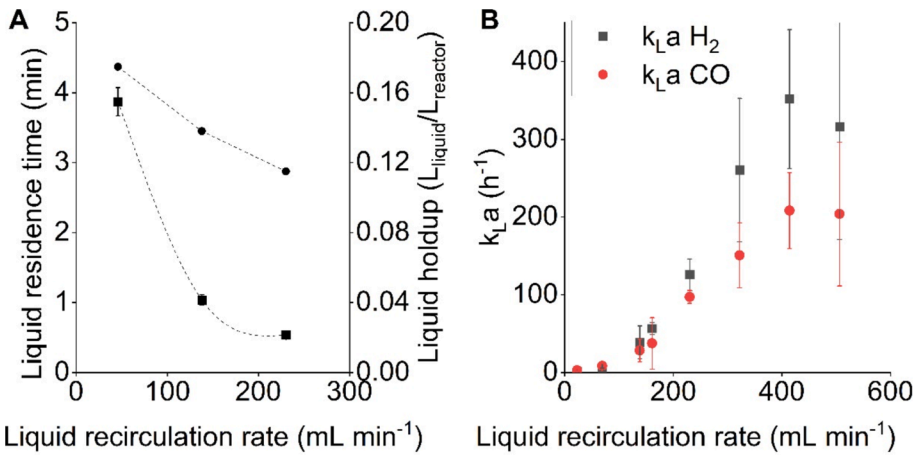

Fig. 4. A) Liquid residence time and liquid holdup (the ratio of liquid volume to total volume) in the trickle bed reactor as a function of liquid recirculation pump flow, and C) volumetric mass transfer coefficient (k_La) of H_2 and CO as a function of the liquid recirculation rate.

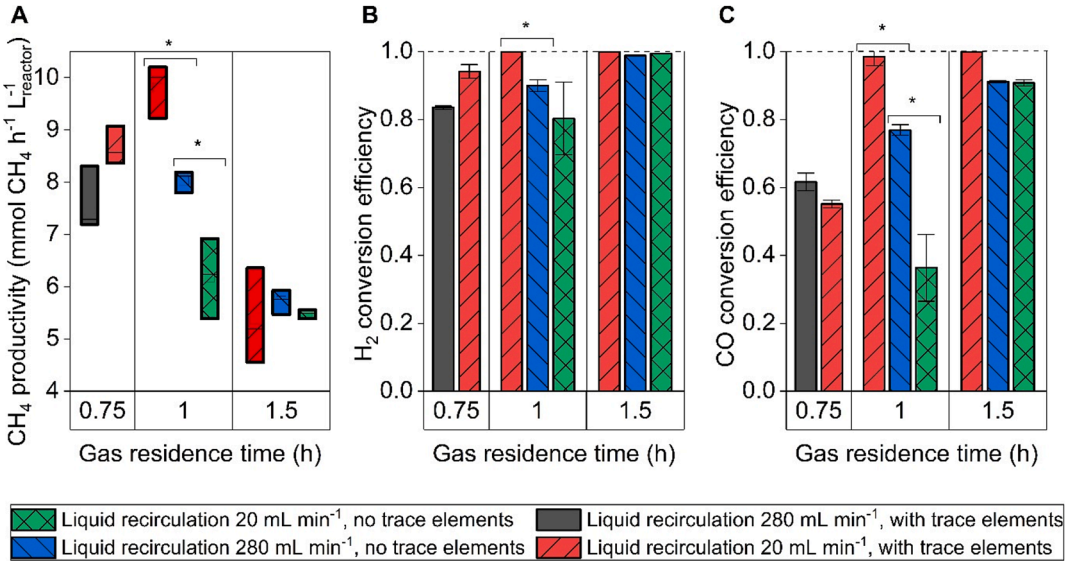

Fig. 5. A) Methane productivity, B) hydrogen conversion efficiency, and C) carbon monoxide conversion efficiency as a function of gas residence time (GRT) for an inlet gas composition of 65 % H_2, 16.7 % CO, 13.1 % CO_2 and 5.2 % N_2. The values are expressed as the average of three consecutive days at steady state and their standard deviation.

presented nearly full conversion of H_2 and CO, and very similar CH_4 productivity. At a GRT of 1 h though, a liquid recirculation rate of 20 mL min^{-1} was insufficient to completely convert the incoming H_2 and CO. Elevating the liquid recirculation rate to 280 mL min^{-1} was expected to improve the productivity and conversion efficiency substantially, since the mass transfer had been improved by an increase in recirculation rate in abiotic conditions. However, the observed results were modest, and nowhere near those expected from the mass transfer coefficient behaviour. The CH_4 productivity did increase significantly (p-value < 0.05), but only by 30 %. There was no significant improvement in H_2 conversion. CO conversion was improved significantly (p-value < 0.05), but full CO conversion was not achieved. This indicated that another factor was limiting the ability of the biofilm to convert syngas to biomethane. This could either be a potential nutrient limitation in the liquid fraction of digestate used as liquid medium, or a different mass transfer related bottleneck like the diffusion of the compounds through the biofilm.

Nutrient limitation can hinder the ability of the biofilm to convert syngas to methane [48]. With an adequate supply of nutrients, a given reactor can convert a larger amount of gas, resulting in higher productivity and conversion efficiency. Thus, trace elements were supplemented to the liquid fraction of digestate used as trickling medium to address any potential nutrient limitation. As shown in Fig. 5A, the supplementation of trace elements resulted in a 59 % increase in CH_4 productivity at a GRT of 1 h, compared to the only 30 % increase achieved by only increasing liquid recirculation. Furthermore, complete H_2 and CO conversion was achieved at GRT 1 h by supplementing trace elements (Fig. 5B and C). Overall, the results show the bottleneck pertaining to the lack of trace elements was overcome and no longer played a role in subsequent experiments.

Once trace element limitation was addressed, the impact of increasing the liquid recirculation rate could be reevaluated. Since trace element supplementation showed complete conversion at a GRT of 1 h even at a 20 mL min^{-1} liquid recirculation rate, the GRT was further lowered to 0.75 h to push the reactor to its maximum possible performance. In this case, neither H_2 nor CO conversion was complete. Furthermore, operation with a liquid recirculation rate of 280 mL min^{-1} did not significantly improve CH_4 productivity nor conversion efficiency. Neither did it greatly affect the uptake rates (see Supplementary Table 1). This indicates that the diffusion of H_2 and CO within the biofilm may be the true rate limiting step of the process, and not the

generally assumed gas–liquid mass transfer. Considering that the biomass in attached to the carriers ranged from 4 to 6 g dry weight and that in the liquid phase ranged between 5 and 10 mg dry weight, biofilm phenomena are likely to contribute significantly to the overall performance of the reactor. Although increasing gas–liquid mass transfer does increase the driving force for diffusion, diffusion is a process several orders of magnitude slower than gas–liquid convective transfer [49], so the effect of increased k_La is not observable in the process performance. This finding carries multiple implications in our understanding of the metabolic network of syngas-converting microbial biofilms (see section 3.3).

The performance obtained in this study compares favourably with values reported in the literature. Asimakopoulos et al. [45] reported a CH_4 productivity of 8.5 mmol $L_{reactor}^{-1}h^{-1}$ with at e-donor/e-acceptor ratio of 2.8 and at a GRT of 0.6 h, with 89 % and 73 % H_2 and CO conversion, respectively. The best performance reported in this work was 9.81 ± 0.52 mmol $L_{reactor}^{-1}h^{-1}$ at a GRT of 1 h, with full H_2 and CO conversion. However, the gas composition requires further H_2 supplementation to achieve a productivity closer to the 17.6 mmol $L_{reactor}^{-1}h^{-1}$ reported for semi-pilot scale [12]. Aside from this last value, the present study finds CH_4 productivities (with full conversion) higher than those previously reported in literature [13,39,50].

3.3. Thermodynamics shape microbial community structure along syngas biomethanation TBRs

Biofilm diffusion was found to be the likely bottleneck of the syngas biomethanation process in TBRs, mirroring the behaviour of similar systems, such as those used in biological wastewater treatment. In wastewater treatment, the diffusion limitation of oxygen and other compounds into and within the biofilm is well established and has been widely studied [19,51,52]. The result is a severe limitation in substrate availability in the biofilm phase. Biofilm communities in TBRs may thus face the challenge of having to scavenge carbon at very low concentrations as the gaseous substrates get consumed along the bed of the reactor, imposing severe bioenergetic restrictions for multiple functional guilds inhabiting the biofilm and ultimately shaping its microbial structure. This hypothesis was investigated analysing the biofilm community structure along the bed of the reactor combined with a thermodynamic analysis of multiple bioenergetically constrained reactions within the metabolic network of syngas-converting microbial communities.

Analysing the microbial composition of the biofilm at three different heights in the reactor showed a clear distribution of different microbial groups along the reactor (Fig. 6B). Having in mind that the gas was supplied from top of the reactor, the largest proportion of reads mapping to hydrogenotrophic methanogens, most notably *Methanothermobacter* and *Methanobacterium* spp., were found at the top of the reactor (Fig. 6B). In turn, carboxydotrophic Firmicutes like *Desulfosporosinus* spp. and *Eubacterium* spp. [43,53,54] became the dominant microbial group at the middle of the reactor, while synergistic bacteria also appeared at the middle of the reactor and their proportion increased towards the bottom of the reactor (Fig. 6C). A Pearson correlation analysis on the relative abundance of the top genera from each phylum showed a clear correlation between several key genera and the height of the reactor (Fig. 6C). *Methanobacterium* spp. was positively correlated with height, which can also clearly be seen in Fig. 6B, in agreement with the H_2 gradient. Acetate consuming genera like *Methanosarcina*, *Syntrophaceticus* and multiple members of the Synergistaceae family [55] were negatively correlated with the height, showing that they were most present at the bottom of the reactor. These observations suggest a high degree of spatial specialisation in the substrate utilisation by the biofilm, where hydrogenotrophic methanogenesis was the dominant at the top of the reactor and was gradually displaced as carboxydotrophs and syntrophic acetate oxidizers increased at the bottom of the reactor. Overall, the microbial community was found to be naturally stratified along the height of the reactor, indicating that the gradient of gaseous substrates along the reactor exerted a strong selective pressure on the biofilm community structure.

The composition of the gas phase along the height of the reactor was studied to validate the above observations. The results were in good agreement with the microbial stratification of the biofilm community as the content of the different gases followed different trends along the height of the reactor. H_2 and CO_2 were mostly consumed at the top of the reactor (Fig. 7B), which concurred with the fact that hydrogenotrophic methanogens were very abundant at the top of the reactor and syntrophic acetate oxidisers barely present. Similarly, the consumption of CO increased at the middle of the reactor, which was in agreement with the dominance of carboxydotrophs at this height (Fig. 7B and 6B). Such dynamics in the gas phase profile and the consistency with the microbial community analysis supported our hypothesis on bioenergetic constraints shaping the biofilm community stratification along the reactor.

The most surprising finding is the presence of syntrophic acetate oxidisers, as the thermodynamic feasibility of their main metabolic reaction is incompatible with the H_2 partial pressure measured in the gas phase. To explore how syntrophic acetate oxidation and hydrogenotrophic methanogenesis could coexist, the thermodynamic potential factors (F_T) of these two reactions were evaluated for a broad range of H_2 and CO_2 concentrations (see Supplementary Figs. 1 and 2). The thermodynamic potential factor gives an indication of the

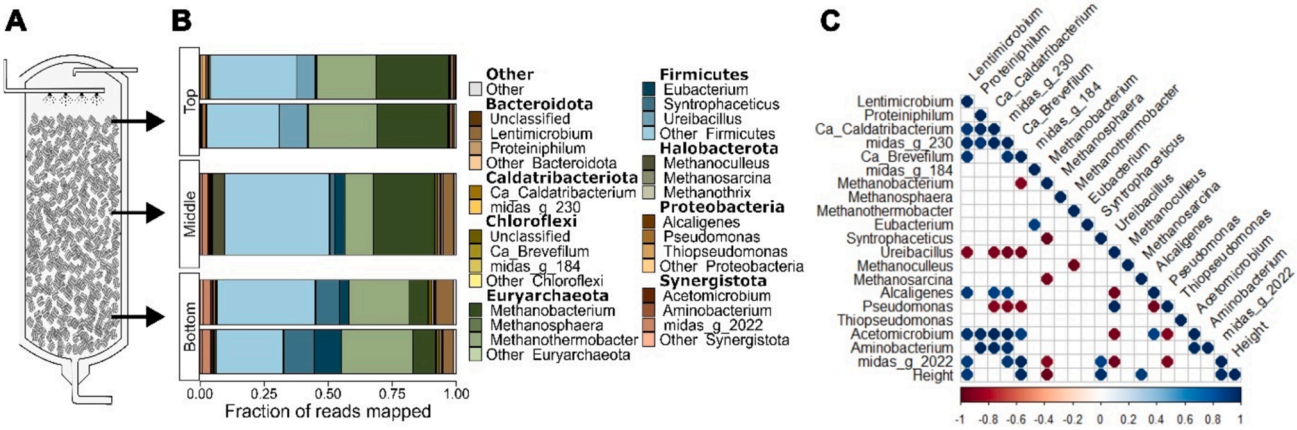

Fig. 6. A) Schematic of the reactor with sampling ports for microbial community analysis, B) the microbial community composition in terms of relative abundance sampled along the height of the reactor, and C) the correlation between the most abundant functionally relevant microbes and the height of the reactor, where only significant (p-value < 0.05) correlations are shown.

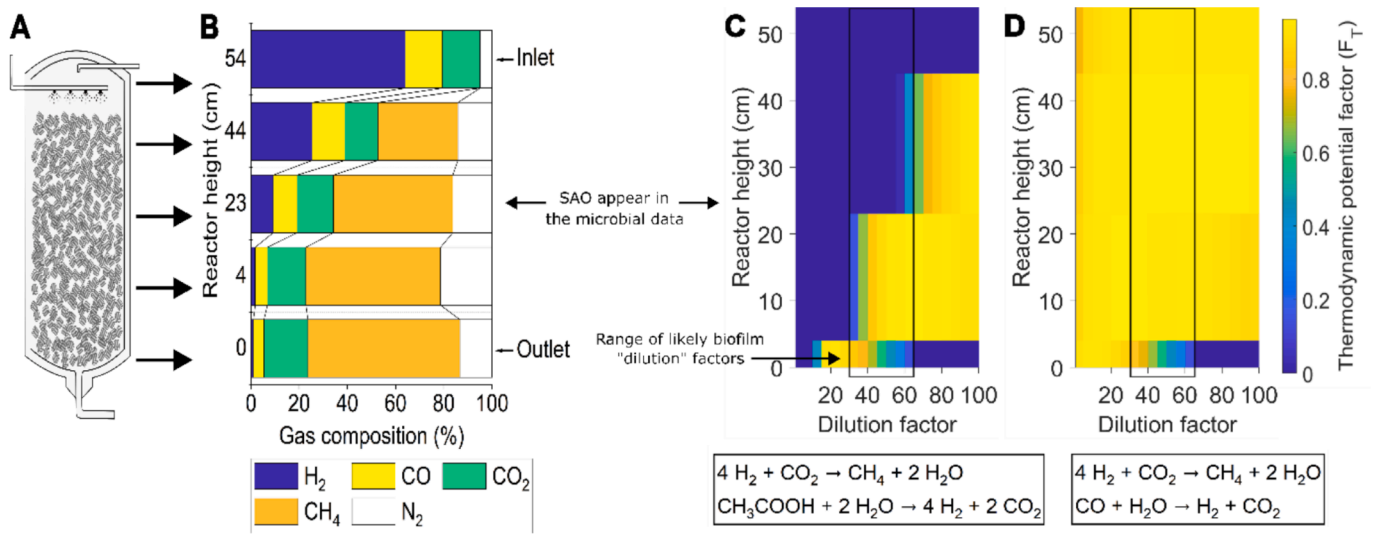

Fig. 7. A) Schematic of the reactor with indications of gas sampling ports, B) profile of gas composition along the height of the reactor, thermodynamic potential factor as a function of height and "dilution factor" of the dissolved concentration in the biofilm for C) hydrogenotrophic methanogenesis ($4\ H_2 + CO_2 \rightarrow CH_4 + 2\ H_2O$) overlapped with syntrophic acetate oxidation ($CH_3COOH + 2\ H_2O \rightarrow 4\ H_2 + 2\ CO_2$), and D) thermodynamic potential factor as a function of height and "dilution factor" for hydrogenotrophic methanogenesis overlapped with carboxydotrophic hydrogenogenesis ($CO + H_2O \rightarrow H_2 + CO_2$). The values shown are average values for three consecutive days at steady state.

thermodynamic drive of a reaction: strong when the factor approaches 1, weakening as it approaches 0. For two reactions to coexist, their thermodynamic potential factors must both be greater than 0. Supplementary Fig. 3 shows the overlap of the concentration range in which both hydrogenotrophic methanogenesis and syntrophic acetate oxidation are feasible ($F_T > 0$). When comparing this range with the liquid phase concentrations calculated from the measured gas concentrations, the reactions were not simultaneously feasible at these dissolved concentrations. This is in discrepancy with the microbial community composition data, where both microbial groups coexist from around the middle of the reactor, with the proportion of syntrophic acetate oxidisers increasing towards the bottom of the reactor. This is a strong indication that, for the two reactions to coexist, the effective concentrations of H_2 needed to be much lower than those calculated in the liquid phase, which is consistent with a mass transfer limitation of transport within the biofilm. As microbial consumption of these compounds is faster than their diffusion into the biofilm, the steady state concentration reached in the biofilm is substantially lower than that in the liquid film [19].

The range of values in Supplementary Fig. 3 where syntrophic acetate oxidation and hydrogenotrophic methanogenesis overlap are up to 100 times lower than those measured in the liquid phase. This range was then used to calculate the thermodynamic potential factor of hydrogenotrophic methanogenesis, carboxydotrophic hydrogenogenesis and syntrophic acetate oxidation over the height of the reactor based on the measured gas concentrations at each of the five sampling ports (see Fig. 1). This profile was calculated for a fraction of the dissolved concentration by dividing it with a "dilution factor" that ranged from 5 to 100. As can be seen in Fig. 7C, the syntrophic acetate oxidation reaction would only become feasible around the middle of the reactor (where syntrophic acetate oxidisers are first observed – Fig. 6C), if the H_2 concentration was at least 35 times lower in the biofilm than in the liquid phase. As their presence is negligible at the top of the reactor, it is unlikely that the H_2 concentration in the biofilm is less than 60 times lower than the liquid phase, as it would make syntrophic acetate oxidation feasible already at the top sampling port of the reactor. Under these diffusion-limited conditions, syntrophic acetate oxidisers could interact with hydrogenotrophic methanogens following an interaction profile very similar to the dynamics of the biofilm composition observed along the bed of the reactor. Their coexistence occurs thanks to the ability of hydrogenotrophic methanogens to scavenge very low concentrations of H_2. In this syntrophic partnership, syntrophic acetate oxidisers produce H_2 from acetate, and the continuation of their activity is ensured by H_2 being consumed by hydrogenotrophic methanogens. These, in turn, are provided with the H_2 and CO_2 required for their metabolism. These results indicate a severe carbon limitation in the biofilm and reinforce the finding that diffusive transport in the biofilm is a key factor in determining both the performance and the microbial structure of the syngas biomethanation reactor.

Carboxydotrophic hydrogenogenesis, for its part, occurs at all heights of the reactor, as can be seen from the gas consumption data (Fig. 7B) and its thermodynamic potential factor overlapped with hydrogenotrophic methanogenesis (Fig. 7D). This behaviour is expected based on the gas composition, which did not have H_2 in excess and does not deviate in the range of biofilm concentrations identified above as most likely.

4. Conclusion

Syngas biomethanation is a complex process involving multiple microbial groups. The sensitivity of this microbiome to high CO supply was minimal, while thermodynamic inhibition by even small excesses in H_2 supply caused drastic process failure. Mass transfer limitations due to diffusive transport of compounds within the biofilm was found to be the most important bottleneck to process performance compared to the commonly assumed gas–liquid mass transfer limitation. This diffusion into the biofilm further shapes which catabolic reactions are possible within the reactor, leading to a spatial substrate-based specialization of the biofilm and stratification of the microbial groups involved in syngas biomethanation.

CRediT authorship contribution statement

Estelle M. Goonesekera: Writing – original draft, Visualization, Methodology, Investigation, Formal analysis, Conceptualization. **Antonio Grimalt-Alemany:** Writing – review & editing, Supervision, Methodology, Formal analysis, Conceptualization. **Eirini Thanasoula:** Investigation. **Hassan F. Yousif:** Investigation. **Sarah L. Krarup:** Investigation. **Maria Chiara Valerin:** Investigation. **Irini Angelidaki:** Writing – review & editing, Supervision, Project administration, Funding acquisition, Conceptualization.

Declaration of competing interest

The authors declare that they have no known competing financial interests or personal relationships that could have appeared to influence the work reported in this paper.

Acknowledgements

This work was financially supported by the European Commission projects SEMPRE-BIO (HORIZON-CL5-2021-D3-03) and CRONUS (HORIZON-CL5-2021-D3-03).

Appendix A. Supplementary data

Supplementary data to this article can be found online at https://doi.org/10.1016/j.cej.2024.156629.

Data availability

Data will be made available on request.

References

[1] S. Paniagua, R. Lebrero, R. Muñoz, Syngas biomethanation: current state and future perspectives, Bioresour. Technol. 358 (2022) 127436, https://doi.org/10.1016/j.biortech.2022.127436.
[2] S. Safarian, R. Unnthorsson, C. Richter, Performance analysis and environmental assessment of small-scale waste biomass gasification integrated CHP in Iceland, Energy 197 (2020) 117268, https://doi.org/10.1016/j.energy.2020.117268.
[3] M. Ellacuriaga, M.V. Gil, X. Gómez, Syngas fermentation: cleaning of syngas as a critical stage in fermentation performance, Fermentation 9 (2023) 898, https://doi.org/10.3390/fermentation9100898.
[4] D. Thrän, T. Persson, J. Daniel-Gromke, J. Ponitka, M. Seiffert, J. Baldwin, L. Kranzl, F. Schipfer, J. Matzenberger, N. Devriendt, M. Dumont, J. Dahl, G. Bochmann, M. Svensson, E. Billig, Biomethane: Status and Factors Affecting Market Development and Trade, in: M. Junginger, D. Baxter (Eds.), Biomethane Status Factors Affect. Mark. Dev. Trade, IEA Bioenergy, 2014. http://www.bioenergytrade.org/publications.html#Biomethane2014, http://www.bioenergytrade.org/downloads/t40-t37-biomethane-2014.pdf.
[5] A. Grimalt-Alemany, I.V. Skiadas, H.N. Gavala, Syngas biomethanation: state-of-the-art review and perspectives, Biofuels Bioprod. Biorefining 12 (2018) 139–158, https://doi.org/10.1002/bbb.1826.
[6] A. Grimalt-Alemany, M. Łężyk, D.M. Kennes-Veiga, I.V. Skiadas, H.N. Gavala, Enrichment of mesophilic and thermophilic mixed microbial consortia for syngas biomethanation: the role of kinetic and thermodynamic competition, Waste Biomass Valorization 11 (2020) 465–481, https://doi.org/10.1007/s12649-019-00595-z.
[7] K.J. Kim, K.W. Jeon, G.R. Hong, B.H. Jeon, J. Wook Bae, W.J. Jang, Y.L. Lee, H. S. Roh, Elucidating the effect of Ce/Zr ratio on high temperature shift activity with sulfur poisoning, J. Ind. Eng. Chem. 115 (2022) 537–543, https://doi.org/10.1016/j.jiec.2022.08.041.
[8] G. Mörsdorf, K. Frunzke, D. Gadkari, O. Meyer, Microbial growth on carbon monoxide, Biodegradation 3 (1992), https://doi.org/10.1007/BF00189635.
[9] S. Sancho Navarro, R. Cimpoia, G. Bruant, S.R. Guiot, Biomethanation of syngas using anaerobic sludge: shift in the catabolic routes with the CO partial pressure increase, Front. Microbiol. 7 (2016), https://doi.org/10.3389/fmicb.2016.01188.
[10] J. Sipma, P.N.L. Lens, A.J.M. Stams, G. Lettinga, Carbon monoxide conversion by anaerobic bioreactor sludges, FEMS Microbiol. Ecol. 44 (2003) 271–277, https://doi.org/10.1016/S0168-6496(03)00033-3.
[11] C. Li, X. Zhu, I. Angelidaki, Carbon monoxide conversion and syngas biomethanation mediated by different microbial consortia, Bioresour. Technol. 314 (2020) 123739, https://doi.org/10.1016/j.biortech.2020.123739.
[12] K. Asimakopoulos, M. Kaufmann-Elfang, C. Lundholm-Høffner, N.B.K. Rasmussen, A. Grimalt-Alemany, H.N. Gavala, I.V. Skiadas, Scale up study of a thermophilic trickle bed reactor performing syngas biomethanation, Appl. Energy 290 (2021) 116771, https://doi.org/10.1016/j.apenergy.2021.116771.
[13] K. Asimakopoulos, A. Grimalt-Alemany, C. Lundholm-Høffner, H.N. Gavala, I. V. Skiadas, Carbon sequestration through syngas biomethanation coupled with H2 supply for a clean production of natural gas grade biomethane, Waste Biomass Valorization 12 (2021) 6005–6019, https://doi.org/10.1007/s12649-021-01393-2.
[14] M. Rivarolo, A.F. Massardo, Optimization of large scale bio-methane generation integrating "spilled" hydraulic energy and pressurized oxygen blown biomass gasification, Int. J. Hydrogen Energy 38 (2013) 4986–4996, https://doi.org/10.1016/j.ijhydene.2013.02.010.
[15] S.M. Techtmann, A.S. Colman, F.T. Robb, 'That which does not kill us only makes us stronger': the role of carbon monoxide in thermophilic microbial consortia, Environ. Microbiol. 11 (2009) 1027–1037, https://doi.org/10.1111/j.1462-2920.2009.01865.x.
[16] K.T. Klasson, M.D. Ackerson, E.C. Clausen, J.L. Gaddy, Bioconversion of synthesis gas into liquid or gaseous fuels, Enzyme Microb. Technol. 14 (1992) 602–608, https://doi.org/10.1016/0141-0229(92)90033-K.
[17] P.C. Munasinghe, S.K. Khanal, Biomass-derived syngas fermentation into biofuels: opportunities and challenges, Bioresour. Technol. 101 (2010) 5013–5022, https://doi.org/10.1016/j.biortech.2009.12.098.
[18] D.E. LaRowe, A.W. Dale, J.P. Amend, P. Van Cappellen, Thermodynamic limitations on microbially catalyzed reaction rates, Geochim. Cosmochim. Acta 90 (2012) 96–109, https://doi.org/10.1016/j.gca.2012.05.011.
[19] H. Horn, E. Morgenroth, Transport of oxygen, sodium chloride, and sodium nitrate in biofilms, Chem. Eng. Sci. 61 (2006) 1347–1356, https://doi.org/10.1016/j.ces.2005.08.027.
[20] M.P. Duduković, Tracer Methods in Chemical Reactors. Techniques and Applications, in: H.I. de Lasa (Ed.), Chem. React. Des. Technol. Overv. New Dev. Energy Petrochem. React. Technol. Proj. 90's, Springer Netherlands, Dordrecht, 1986: pp. 107–189. https://doi.org/10.1007/978-94-009-4400-8_5.
[21] W. APHA, Standard methods for the examination of water and wastewater, American Public Health Association, 2005. https://www.apha.org/.
[22] G. Giangeri, P. Tsapekos, M. Gaspari, P. Ghofrani-Isfahani, L. Treu, P. Kougias, S. Campanaro, I. Angelidaki, A bioaugmentation strategy to recover methane production under sulfate-stressed conditions: highlights on targeted sulfate-reducing bacteria and DIET-related species, Appl. Energy 362 (2024) 122940, https://doi.org/10.1016/j.apenergy.2024.122940.
[23] P.G. Kougias, L. Treu, D.P. Benavente, K. Boe, S. Campanaro, I. Angelidaki, *Ex-situ* biogas upgrading and enhancement in different reactor systems, Bioresour. Technol. 225 (2017) 429–437, https://doi.org/10.1016/j.biortech.2016.11.124.
[24] J.G. Caporaso, C.L. Lauber, W.A. Walters, D. Berg-Lyons, C.A. Lozupone, P. J. Turnbaugh, N. Fierer, R. Knight, Global patterns of 16S rRNA diversity at a depth of millions of sequences per sample, Proc. Natl. Acad. Sci. 108 (2011) 4516–4522, https://doi.org/10.1073/pnas.1000080107.
[25] M. Martin, Cutadapt removes adapter sequences from high-throughput sequencing reads, EMBnet J. 17 (2011) 10–12, https://doi.org/10.14806/ej.17.1.200.
[26] E. Bolyen, et al., Reproducible, interactive, scalable and extensible microbiome data science using QIIME 2, Nat. Biotechnol. 37 (2019) 852–857, https://doi.org/10.1038/s41587-019-0209-9.
[27] M.K.D. Dueholm, M. Nierychlo, K.S. Andersen, V. Rudkjøbing, S. Knutsson, M. Albertsen, P.H. Nielsen, MiDAS 4: A global catalogue of full-length 16S rRNA gene sequences and taxonomy for studies of bacterial communities in wastewater treatment plants, Nat. Commun. 13 (2022) 1908, https://doi.org/10.1038/s41467-022-29438-7.
[28] P.J. McMurdie, S. Holmes, phyloseq: An R package for reproducible interactive analysis and graphics of microbiome census data, PLoS One 8 (2013) e61217, https://doi.org/10.1371/journal.pone.0061217.
[29] J. Oksanen, G.L. Simpson, F.G. Blanchet, R. Kindt, P. Legendre, P.R. Minchin, R.B. O'Hara, P. Solymos, M.H.H. Stevens, E. Szoecs, H. Wagner, M. Barbour, M. Bedward, B. Bolker, D. Borcard, G. Carvalho, M. Chirico, M.D. Caceres, S. Durand, H.B.A. Evangelista, R. FitzJohn, M. Friendly, B. Furneaux, G. Hannigan, M.O. Hill, L. Lahti, D. McGlinn, M.-H. Ouellette, E.R. Cunha, T. Smith, A. Stier, C.J.F.T. Braak, J. Weedon, vegan: Community Ecology Package, 2024. https://github.com/veganevs/vegan.
[30] A. Kassambara, ggpubr: "ggplot2" Based Publication Ready Plots, 2023. https://rpkgs.datanovia.com/ggpubr/.
[31] R Core Team, R: A Language and Environment for Statistical Computing, (2023). {https://www.R-project.org/}.
[32] Q. Jin, C.M. Bethke, The thermodynamics and kinetics of microbial metabolism, Am. J. Sci. 307 (2007) 643–677, https://doi.org/10.2475/04.2007.01.
[33] R.A. Alberty, Thermodynamics of Biochemical Reactions, Wiley-Interscience, Hoboken, NJ, 2003.
[34] A.-K. Kaster, J. Moll, K. Parey, R.K. Thauer, Coupling of ferredoxin and heterodisulfide reduction via electron bifurcation in hydrogenotrophic methanogenic archaea, Proc. Natl. Acad. Sci. 108 (2011) 2981–2986, https://doi.org/10.1073/pnas.1016761108.
[35] A. Grimalt-Alemany, K. Asimakopoulos, I.V. Skiadas, H.N. Gavala, Modeling of syngas biomethanation and catabolic route control in mesophilic and thermophilic mixed microbial consortia, Appl. Energy 262 (2020) 114502, https://doi.org/10.1016/j.apenergy.2020.114502.
[36] H.J. van Lingen, C.M. Plugge, J.G. Fadel, E. Kebreab, A. Bannink, J. Dijkstra, Thermodynamic driving force of hydrogen on rumen microbial metabolism: a theoretical investigation, PLoS One 11 (2016) e0161362, https://doi.org/10.1371/journal.pone.0161362.
[37] S. Benito-Vaquerizo, I. Parera Olm, T. de Vroet, P.J. Schaap, D.Z. Sousa, V.A. P. Martins dos Santos, M. Suarez-Diez, Genome-scale metabolic modelling enables deciphering ethanol metabolism via the acrylate pathway in the propionate-producer Anaerotignum neopropionicum, Microb. Cell Factories 21 (2022) 116, https://doi.org/10.1186/s12934-022-01841-1.
[38] B.E. Jackson, M.J. McInerney, Anaerobic microbial metabolism can proceed close to thermodynamic limits, Nature 415 (2002) 454–456, https://doi.org/10.1038/415454a.
[39] G. Cheng, F. Gabler, L. Pizzul, H. Olsson, Å. Nordberg, A. Schnürer, Microbial community development during syngas methanation in a trickle bed reactor with various nutrient sources, Appl. Microbiol. Biotechnol. 106 (2022) 5317–5333, https://doi.org/10.1007/s00253-022-12035-5.
[40] S.N. Parshina, S. Kijlstra, A.M. Henstra, J. Sipma, C.M. Plugge, A.J.M. Stams, Carbon monoxide conversion by thermophilic sulfate-reducing bacteria in pure culture and in co-culture with Carboxydothermus hydrogenoformans, Appl.

Microbiol. Biotechnol. 68 (2005) 390–396, https://doi.org/10.1007/s00253-004-1878-x.
[41] J. Figueras, H. Benbelkacem, C. Dumas, P. Buffiere, Syngas biomethanation: In a transfer limited process, is CO inhibition an issue? Waste Manag. 162 (2023) 36–42, https://doi.org/10.1016/j.wasman.2023.03.011.
[42] Q. Jin, Energy conservation of anaerobic respiration, Am. J. Sci. 312 (2012) 573–628, https://doi.org/10.2475/06.2012.01.
[43] F.R. Bengelsdorf, M.H. Beck, C. Erz, S. Hoffmeister, M.M. Karl, P. Riegler, S. Wirth, A. Poehlein, D. Weuster-Botz, P. Dürre, Bacterial Anaerobic Synthesis Gas (Syngas) and CO 2 + H 2 Fermentation, in: Adv. Appl. Microbiol., Elsevier, 2018: pp. 143–221. https://doi.org/10.1016/bs.aambs.2018.01.002.
[44] S.N. Parshina, J. Sipma, A.M. Henstra, A.J.M. Stams, Carbon monoxide as an electron donor for the biological reduction of sulphate, Int. J. Microbiol. 2010 (2010) 319527, https://doi.org/10.1155/2010/319527.
[45] K. Asimakopoulos, H.N. Gavala, I.V. Skiadas, Biomethanation of syngas by enriched mixed anaerobic consortia in trickle bed reactors, Waste Biomass Valorization 11 (2020) 495–512, https://doi.org/10.1007/s12649-019-00649-2.
[46] M.D. Bredwell, P. Srivastava, R.M. Worden, Reactor design issues for synthesis-gas fermentations, Biotechnol. Prog. 15 (1999) 834–844, https://doi.org/10.1021/bp990108m.
[47] J.-C. Charpentier, Mass-Transfer Rates in Gas-Liquid Absorbers and Reactors, in: Adv. Chem. Eng., Elsevier, 1981: pp. 1–133. https://doi.org/10.1016/S0065-2377(08)60025-3.
[48] F. Ebrahimian, G. Lovato, M. Alvarado-Morales, M.T. Ashraf, J.A.D. Rodrigues, P. Tsapekos, I. Angelidaki, Iron limitation effect on H_2/CO_2 biomethanation: experimental and model analysis, J. Environ. Chem. Eng. 11 (2023) 109529, https://doi.org/10.1016/j.jece.2023.109529.
[49] J.-H. Wang, H.-Y. Li, Y.-P. Chen, S.-Y. Liu, P. Yan, Y. Shen, J.-S. Guo, F. Fang, Estimation of oxygen effective diffusion coefficient in a non-steady-state biofilm based on response time, Environ. Sci. Pollut. Res. 25 (2018) 9797–9805, https://doi.org/10.1007/s11356-018-1227-8.
[50] J. Figueras, H. Benbelkacem, C. Dumas, P. Buffiere, Biomethanation of syngas by enriched mixed anaerobic consortium in pressurized agitated column, Bioresour. Technol. 338 (2021) 125548, https://doi.org/10.1016/j.biortech.2021.125548.
[51] X. Guimerà, A.D. Dorado, A. Bonsfills, G. Gabriel, D. Gabriel, X. Gamisans, Dynamic characterization of external and internal mass transport in heterotrophic biofilms from microsensors measurements, Water Res. 102 (2016) 551–560, https://doi.org/10.1016/j.watres.2016.07.009.
[52] T.C. Zhang, P.L. Bishop, Evaluation of tortuosity factors and effective diffusivities in biofilms, Water Res. 28 (1994) 2279–2287, https://doi.org/10.1016/0043-1354(94)90043-4.
[53] B.R.S. Genthner, M.P. Bryant, Growth of Eubacterium limosum with carbon monoxide as the energy source, Appl. Environ. Microbiol. 43 (1982) 70–74.
[54] O. Meyer, K. Fiebig. Enzymes Oxidizing Carbon Monoxide, in: H. Degn, R.P. Cox, H. Toftlund (Eds.), Gas Enzymol., Springer Netherlands, Dordrecht, 1985: pp. 147–168. https://doi.org/10.1007/978-94-009-5279-9_11.
[55] M. Jetten, A. Stams, A. Zehnder, Methanogenesis from acetate - a comparison of the acetate metabolism in Methanothrix-Soehngenii and Methanosarcina spp, FEMS Microbiol. Lett. 88 (1992) 181–197, https://doi.org/10.1016/0378-1097(92)90802-U.